

## Transfer probabilities for the reactions $^{14,20}\text{O} + ^{20}\text{O}$ in terms of multiple time-dependent Hartree-Fock-Bogoliubov trajectories

Guillaume Scamps\* and Yukio Hashimoto†

Center for Computational Sciences, University of Tsukuba, Tsukuba 305-8571, Japan

(Received 7 August 2017; published 27 September 2017)

The transfer reaction between two nuclei in the superfluid phase is studied with the time-dependent Hartree-Fock-Bogoliubov (TDHFB) theory. To restore the symmetry of the relative gauge angle, a set of independent TDHFB trajectories is taken into account. Then, the transfer probability is computed using a triple projection method. This method is first tested to determine the transfer probabilities on a toy model and compared to the exact solution. It is then applied to the reactions  $^{20}\text{O} + ^{20}\text{O}$  and  $^{14}\text{O} + ^{20}\text{O}$  in a realistic framework with a Gogny interaction.

DOI: 10.1103/PhysRevC.96.031602

**Introduction.** During the last decade, realistic calculations of time-dependent mean-field simulations have been developed including pairing correlations. The first time-dependent Hartree-Fock-Bogoliubov (TDHFB) calculation was carried out by using a spatial lattice assuming spherical symmetry [1]. Then, three-dimensional (3D) calculations with the BCS approximation for the pairing were performed [2–4]. The development of full 3D TDHFB calculations with no spatial symmetries has also been achieved [5,6]. The hybrid basis method has permitted the conception of a TDHFB calculation with Gogny interactions [7,8].

Despite this progress, dynamical mean-field calculations suffer from the problem of the classical trajectory of collective variables. It is for example impossible to describe tunneling in fusion or fission reactions. For fission, the time-dependent generator coordinate method (TDGCM) [9–11] solves partially this problem but assumes a collective motion in a space of adiabatic basis. On the other hand, for fusion tunneling, the density-constraint Hartree-Fock [12,13] is restrained to a single energy-dependent fusion path.

Another example of the limitation of time-dependent mean-field calculation is the lack of fluctuation, due to the consideration of only one quasiparticle vacuum state to describe a reaction. With the aim of curing the problem and getting over the limitations, the time-dependent random-phase approximation (TDRPA) [14–17] or the stochastic mean field (SMF) [18–21] are interesting directions. We can note in particular, the recent article [22] that describes fission with an ensemble of TDHF+BCS trajectories with different initial densities determined randomly. The observables after the scission are computed as the average value over the statistical ensemble of trajectories. In that case, the quantal fluctuations are supposed to behave like statistical fluctuations.

In the present approach, we consider the evolution of a state that is a mixture of several TDHFB states (trajectories). In a previous contribution, we showed that the fusion dynamics [8] changes with the initial relative gauge angle. In addition, being analogous with the well-known Josephson effect, the

nucleus-nucleus potential contains a non-negligible pairing contribution that varies with the gauge angle of the two fragments. This has been confirmed for heavier nuclei [23,24], where it is shown that the solitonic excitation due to the gauge angle difference can change the barrier height by several MeV.

As discussed in Ref. [25], when we treat a case in which two superfluid objects are close to each other and exchange pairs of particles between them, it is necessary to project on the initial particle difference number. This gives us an ideal test case to investigate the evolution of projected states in which various gauge angles are mixed at the initial time.

A projection method to compute the transfer probability in a time-dependent mean-field calculation has been proposed in Ref. [26]. It has been used to make realistic prediction of the cross section in multinucleon transfer reactions [27]. The method has been generalized for calculation where one of the fragment is in the superfluid phase [4]. This method can be used to understand the excitation energy in a transfer channel [28,29]. In this contribution, we use the mixing of TDHFB trajectories to compute the transfer probabilities in reactions where both fragments are initially superfluid. In this article, the projection method is first described and tested with a simple toy model and then it is applied to a realistic model.

**Method.** Here we test the projection method by using a simple toy model. We have two systems, left (L) and right (R), which are composed of  $\Omega$  levels, each of which is doubly degenerate. The two systems are separately initialized with the following Hamiltonian:

$$\hat{H}_0 = \sum_{i>0} h_i (\hat{a}_i^\dagger \hat{a}_i + \hat{a}_{\bar{i}}^\dagger \hat{a}_{\bar{i}}) + G \sum_{i \neq j} \hat{a}_i^\dagger \hat{a}_{\bar{i}}^\dagger \hat{a}_{\bar{j}} \hat{a}_j, \quad (1)$$

with mean-field energy  $h_i = i$  MeV with  $i = 1$  to  $\Omega$ . It is assumed in this model that all the particles are paired. The HFB method is used to determine the ground states of the two systems with a constraint to have  $N_L^0$  ( $N_R^0$ ) particles in the left (right) system. Then, to simulate a collision, an HFB state  $|\phi(t=0)\rangle$  of a set of the two systems is constructed from the two quasiparticle vacuum states.

From this HFB state that breaks the exact conservation of the particle number, a projected state is initially created,

$$|\Psi(t=0)\rangle = \hat{P}_L(N_L^0) |\phi(t=0)\rangle, \quad (2)$$

\*scamps@nucl.ph.tsukuba.ac.jp

†hashimoto.yukio.gb@u.tsukuba.ac.jp

where  $\hat{P}_L(N_L^0)$  is a projector to a state with  $N_L^0$  particles in the left system,

$$\hat{P}_L(N_L^0) = \frac{1}{2\pi} \int_0^{2\pi} e^{i\varphi(\hat{N}_L - N_L^0)} d\varphi. \quad (3)$$

This projection is made to restore the symmetry with respect to the relative gauge angle. We chose arbitrarily to project initially on the left, but a projection on the right or on the initial difference of number of particles would lead to the same results. The integral is discretized with the Fomenko method [30], with  $M$  points,

$$|\Psi(t=0)\rangle = \frac{1}{M} \sum_{n=1}^M e^{-i\frac{2n\pi}{M}N_L^0} |\phi_n(t=0)\rangle, \quad (4)$$

and

$$|\phi_n(t=0)\rangle = e^{i\frac{2n\pi}{M}\hat{N}_L} |\phi(t=0)\rangle. \quad (5)$$

The initial state is then a mixing of  $M$  HFB states with different initial relative gauge angles. In the toy model, the transfer of particles is induced by a time-dependent coupling between the two systems that is assumed to be Gaussian as a function of time. Then, the total Hamiltonian of the system is written as the sum of the initial left  $\hat{H}_0^{(L)}$  and right  $\hat{H}_0^{(R)}$  Hamiltonians and a coupling term,

$$\hat{H}(t) = \hat{H}_0^{(L)} + \hat{H}_0^{(R)} + V(t) \sum_{i \in L; j \in R} (\hat{a}_i^\dagger \hat{a}_i^\dagger \hat{a}_j \hat{a}_j + \hat{a}_j^\dagger \hat{a}_j^\dagger \hat{a}_i \hat{a}_i), \quad (6)$$

with

$$V(t) = V_0 e^{-at^2}. \quad (7)$$

The natural way of performing this calculation would be to derive the equation of motion from the minimization of the action of the evolution of the projected system. Nevertheless, this method would require us to compute the matrix elements of the Hamiltonian matrix, which would lead to spurious results with the use of the density-dependent effective interaction [31].

Then, in this calculation, we assume that the form of the mixing [Eq. (4)] does not change as a function of time,

$$|\Psi(t)\rangle = \frac{1}{M} \sum_{n=1}^M e^{-i\frac{2n\pi}{M}N_L^0} |\phi_n(t)\rangle, \quad (8)$$

and that every HFB state evolves independently with the following TDHFB equation of motion,

$$i\hbar \frac{\partial}{\partial t} \begin{pmatrix} U_k(t) \\ V_k(t) \end{pmatrix} = \mathcal{H}_k(t) \begin{pmatrix} U_k(t) \\ V_k(t) \end{pmatrix}, \quad (9)$$

with

$$\mathcal{H}_k(t) = \begin{pmatrix} h - \delta\lambda_{L,R} - \epsilon_k & \Delta \\ -\Delta^* & -h^* + \delta\lambda_{L,R} - \epsilon_k \end{pmatrix}. \quad (10)$$

with  $\epsilon_k(t)$  the quasiparticle energy.

The  $\delta\lambda_{L,R}(t)$  variable is defined as the difference  $\lambda_{L,R}(t) - \lambda_{L,R}(t=0)$ . The chemical potential  $\lambda_L$  ( $\lambda_R$ ) in the left (right) subspace is introduced to avoid phase rotation among TDHFB states [32],

$$\lambda_{L,R} = \text{Real} \left( \frac{\sum_{i \in L,R} \kappa_{i\bar{i}} M_{i\bar{i}}}{\sum_{i \in L,R} \kappa_{i\bar{i}}} \right), \quad (11)$$

with the  $M_{i\bar{i}}$  matrix,

$$M_{i\bar{i}} = \frac{1}{\kappa_{i\bar{i}}} \left[ \frac{1}{2} h \kappa + \kappa h^* - \Delta \rho^* + (1 - \rho) \Delta \right]_{i\bar{i}}. \quad (12)$$

The  $\delta\lambda_{L,R}(t)$  is equal to  $\delta\lambda_L(t)$  for  $z < 0$  and  $\delta\lambda_R(t)$  for  $z > 0$ . The phase rotation in the process of the TDHFB evolution would induce a spurious time dependence of the results after the transfer as we can see in Fig. 5.

The main observables of interest here are the transfer probabilities. To calculate them, we use a projection method [26] to determine the probability  $P_{L,R}(N,t)$  to obtain  $N$  particles in the left or right part of the system at the time  $t$ ,

$$P_{L,R}(N,t) = \langle \Psi(t) | \hat{P}_{L,R}(N) | \Psi(t) \rangle. \quad (13)$$

As shown in Ref. [4], in a theoretical framework in which the many-body states mix different total number of particles, it is necessary to select the components that contain the good total number of particles. Here, we have projected initially on the good initial number on the left [see Eq. (2)]. In addition, we needed to project on the total number of particles  $N_{\text{tot}} = N_L + N_R$  before making a measurement on the system,

$$\begin{aligned} P_{L,R}(N,t) &= \frac{1}{\mathcal{N}} \langle \Psi(t) | \hat{P}_{L,R}(N) \hat{P}(N_{\text{tot}}) | \Psi(t) \rangle, \\ &= \frac{1}{M^2 \mathcal{N}} \sum_{n,m} e^{i\frac{2(n-m)\pi}{M}N_L^0} \langle \phi_n(t) | \hat{P}_{L,R}(N) \hat{P}(N_{\text{tot}}) | \phi_m(t) \rangle. \end{aligned} \quad (14)$$

Here,  $\mathcal{N}$  is the norm,

$$\mathcal{N} = \langle \Psi(t) | \hat{P}(N_{\text{tot}}) | \Psi(t) \rangle, \quad (16)$$

and  $\hat{P}(N_{\text{tot}})$  the particle number projector on the total number  $N_{\text{tot}} = N_L^0 + N_R^0$ .

Note that the projection  $\hat{P}(N_{\text{tot}})$  can also be made at the initial time and so added into Eq. (2). But these would not change the evolution since the TDHFB equations are independent of a rotation of the gauge angle associated with the total number of particles.

To compute the overlaps in Eq. (15), we develop, respectively, the projector  $\hat{P}_{L,R}(N)$  and  $\hat{P}(N_{\text{tot}})$  as integral with respect to the gauge angle  $\varphi_1$  and  $\varphi_2$ . Then, we use the Pfaffian method [33] to compute,

$$\begin{aligned} \langle \phi_n(t) | e^{i\varphi_2 \hat{N}_{L,R}} e^{i\varphi_3 \hat{N}_{\text{tot}}} | \phi_m(t) \rangle &= (-1)^{n_{\text{qp}}} \frac{\det C^* \det C'}{\prod_{\alpha}^n v_{\alpha} v'_{\alpha}} \\ &\times \text{pf} \begin{bmatrix} V^T U & V^T e^{i\varphi_3} [1 + \Theta_{L,R}(\vec{r})] V^{*} \\ -V'^{\dagger} e^{i\varphi_3} [1 + \Theta_{L,R}(\vec{r})] (e^{i\varphi_2} - 1) V & U'^{\dagger} V'^* \end{bmatrix}. \end{aligned} \quad (17)$$

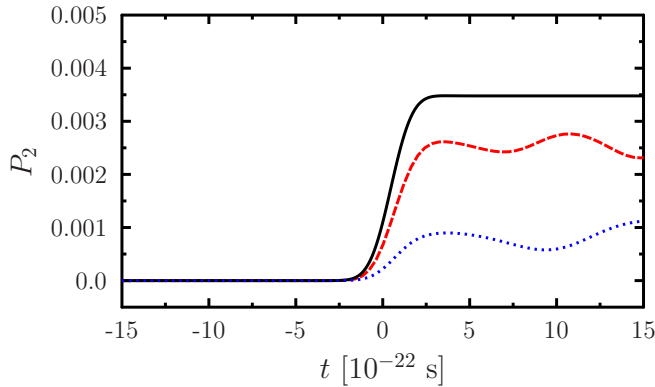


FIG. 1. Pair transfer probability as a function of time in the toy model. Calculations by the present method with (red dashed curve) and without (dotted blue line) an effective interaction are compared to the exact solution (black solid curve).

Here,  $C$ ,  $v_\alpha$ ,  $V$ , and  $U$  correspond to the bra  $\langle \phi_n(t) |$  while the  $C'$ ,  $v'_\alpha$ ,  $V'$ , and  $U'$  refer to the ket  $|\phi_m(t)\rangle$ . The matrices  $C$  and  $C'$  are obtained from the Bloch-Messiah decomposition [34].  $v_\alpha$  and  $v'_\alpha$  are the occupation numbers in the canonical basis and  $n_{qp}$  is the number of quasiparticle states. The Heaviside function  $\Theta_L(\vec{r})$  ( $\Theta_R(\vec{r})$ ) is equal to one in the left (right) part of the system.

To test our present method, we make a comparison with the exact solution of the many-body problem. The exact solution is obtained first by diagonalization of the Hamiltonian in the space of all the possible configurations and then by solving the time-dependent Schrödinger equation. In the Hamiltonian Eq. (6), we use the following parameters:  $\Omega = 4$ ,  $N_L^0 = N_R^0 = 4$ ,  $G = -1$  MeV,  $V_0 = -0.03$  MeV, and  $a = 0.3 \times 10^{44}$  s $^{-2}$ . The calculation is carried out between the time  $t_i = -15 \times 10^{-22}$  s until  $t_f = 15 \times 10^{-22}$  s. Two calculations are carried out, one with the above parameters and one where the interaction constants  $G$  and  $V_0$  are multiplied by 1.475 in the HFB and TDHFB calculations in order to obtain an effective interaction that reproduces the initial exact energy.

The use of a Gaussian-type coupling as a function of time allowed us to mimic the reactions. Initially at  $t = t_i$ , there is no coupling between the two systems. Then, around  $t = 0$  the two systems interact via the pairing interaction and can exchange pairs. At the final time  $t = t_f$ , the systems are isolated from each other. The results as a function of time are shown in Fig. 1. The transfer takes place in the vicinity of  $t = 0$ . After  $t = 3 \times 10^{-22}$  s, the transfer probability is constant in the exact case while small oscillations occur in the TDHFB result. This phenomenon is due to the choice of the approximations made in the calculation which is based on an assumption that the TDHFB trajectories in the state  $|\Psi(t)\rangle$  are independent of each other. Nevertheless, the averaged value of the transfer probability as a function of time is close to the exact solution with the use of the effective interaction. As we can see in Fig. 1, the use of the effective interaction increases the pair transfer by a factor of 3. The use of an effective interaction is justified here because the evolution of the system is made by a set of TDHFB calculations. In each trajectory, the transfer of a pair by the Josephson effect is governed by the pairing field

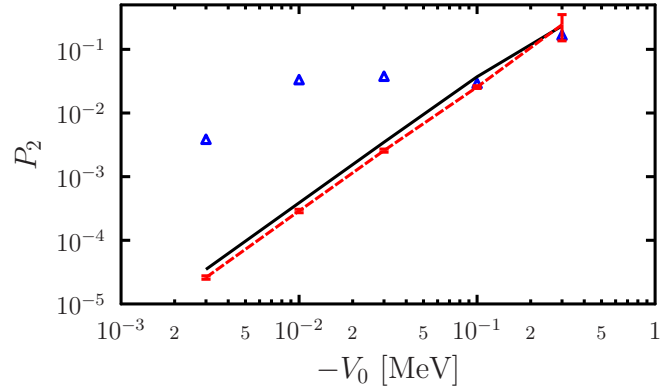


FIG. 2. Pair transfer probability as a function of the strength  $V_0$  of the transfer coupling in the Hamiltonian (6). Calculation by the present method with the effective interaction (red dashed curve) is compared to the exact solution (black solid curve). The blue triangles represent the results obtained without the chemical potential and quasiparticle energy correction at an arbitrary time of  $50 \times 10^{-22}$  s. The error bars on the red curve represent the standard deviation of the probabilities as a function of time after the reaction.

$\Delta$ . To obtain a correct result, the interaction strength should be increased in order to compensate for the lack of correlations due to the HFB approximation. This is simply realized by adjusting the interaction strength by using the same factor as is used to reproduce the ground state energy which also varies with  $\Delta$ .

With the purpose of illustrating the relation between the averaged value of the transfer probability in the TDHFB case and that in the exact case, we plot the pair transfer probability as a function of the strength of the transfer coupling in Fig. 2. The error bars represent the standard deviation of the probabilities as a function of time after the reaction (here for time,  $t > 3 \times 10^{-22}$  s). We see that the TDHFB results reproduce well the exact solution when the interaction strength is varied in several orders of magnitude. To show the importance of the prescription concerning the modification of the TDHFB equation [Eq. (10)] we show pair transfer probability at a large time of  $50 \times 10^{-22}$  s. We see that the transfer probabilities are overestimated by two orders of magnitudes compared with the results of the calculations with the present prescription as well as the exact cases.

In this way, the results of the calculation in the toy model illustrate that the present method works well and we could expect that it has a predictive power in the realistic TDHFB calculations.

*Realistic calculations.* To make the calculation with a realistic interaction, we use the Gogny TDHFB code that uses a hybrid basis. The quasiparticle vacuum states of the two oxygen nuclei are separately initialized and then put in the same lattice with a boost. The method to form the initial HFB state  $|\phi(t=0)\rangle$  is described in Ref. [8].

The Gogny D1S effective interaction was used in the calculations presented below. The projector in Eq. (4) is discretized with eight sampling points  $M = 8$ . Using the symmetry property, only the first four gauge angles are used.

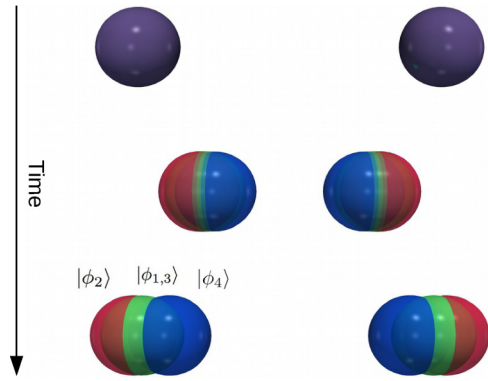


FIG. 3. Superposition of the isodensity surfaces at  $\rho = 0.8 \text{ fm}^{-3}$  as a function of time for the reaction  $^{20}\text{O} + ^{20}\text{O}$  with the center-of-mass energy  $E_{\text{c.m.}} = 9.31 \text{ MeV}$ . The red and blue surfaces are respectively computed from the state  $|\phi_2\rangle$  and  $|\phi_4\rangle$  while the green surface is computed from the states  $|\phi_1\rangle$  and  $|\phi_3\rangle$ .

We calculated a test case with the sampling points  $M = 16$  and found that there is practically no difference in the numerical results below between the cases with  $M = 8$  and  $M = 16$ . The projectors at the final time are discretized with 16 points.

The evolution of TDHFB trajectories with four different gauge angles is shown in Fig. 3. After the reaction, there is a splitting among the trajectories that is due to the dependence of the nucleus-nucleus potential on the initial gauge angle [8]. The trajectory of  $|\phi_2\rangle$  corresponding to a relative gauge angle of  $\varphi = 90^\circ$  is the one with the highest barrier and so the smallest contact time. The opposite case is  $\varphi = 0^\circ$  ( $|\phi_4\rangle$ ) with the largest contact time.

This effect, which gives rise to the splitting among the trajectories, changes the overlap as a function of time. As we can see in Fig. 4, the overlap  $|\langle\phi_1(t)|\phi_2(t)\rangle|^2$  is constant until the contact, then the overlap drops to zero because the trajectories diverge. So the probabilities, in a similar way as the phase rotation, change as a function of time. We can see in Fig. 5, that the direct application of the method (purple dashed line) leads to a very large pair transfer probability that is not stabilized after the reaction. To solve this problem, we introduce a prescription to compensate for the dispersion of the

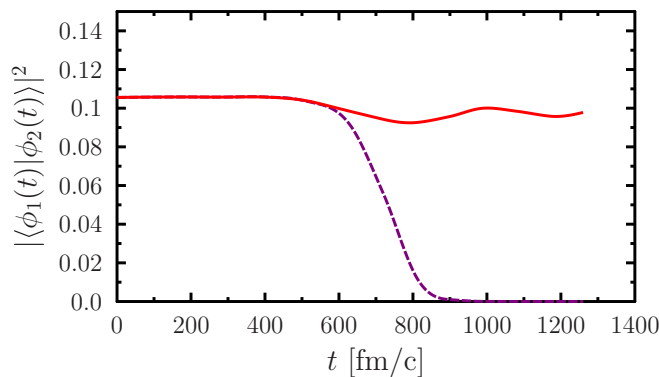


FIG. 4. Norm of the overlap between states 1 and 2 (respectively  $\varphi = 0^\circ$  and  $45^\circ$ ) as a function of time, with (red solid line) and without (purple dashed line) the center-of-mass shift.

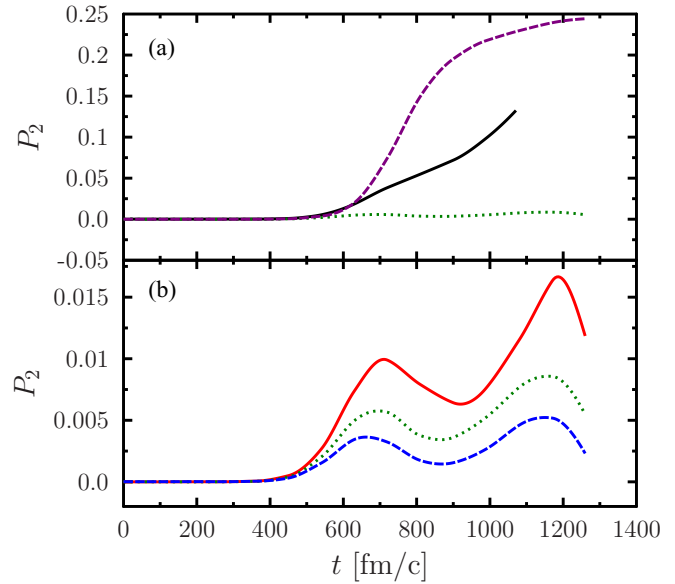


FIG. 5. Pair transfer probability as a function of time for the reaction  $^{20}\text{O} + ^{20}\text{O}$ . (a) TDHFB calculation without center-of-mass shift (purple dashed line), without the chemical potential and quasi-particle energy correction (solid line), and the correct calculation at the center-of-mass energy  $E_{\text{c.m.}} = 9.21 \text{ MeV}$  (green dotted line). (b) Corrected calculation at  $E_{\text{c.m.}} = 9.31 \text{ MeV}$  (red solid line),  $E_{\text{c.m.}} = 9.21 \text{ MeV}$  (green dotted line), and  $E_{\text{c.m.}} = 8.91 \text{ MeV}$  (blue dashed line).

trajectories. We artificially shift the position of each fragment of the ket  $|\phi_m(t)\rangle$  to have the same center of mass of the bra  $\langle\phi_n(t)|$ ,

$$U'(\vec{r}) \rightarrow U''(\vec{r}) = U'(\vec{r} - \vec{d}_{L,R}), \quad (18)$$

$$V'(\vec{r}) \rightarrow V''(\vec{r}) = V'(\vec{r} - \vec{d}_{L,R}), \quad (19)$$

with  $\vec{d}_{L,R}$  the difference of position between the bra and the ket in the left or right part of the lattice,  $\vec{d}_{L,R} = \vec{R}_{L,R} - \vec{R}'_{L,R}$ .  $\vec{R}_{L,R}$  ( $\vec{R}'_{L,R}$ ) is the center-of-mass position in the left or the right of the system associated with the bra (ket). With this prescription, we ensure that there is no diminution of the overlap after the separation of the fragments.

It is also necessary to take into account this shift of the position in the calculation of the chemical potential. The matrix  $M_{i\bar{i}}$  in Eq. (12) is changed into

$$M_{i\bar{i}} = \frac{1}{\kappa_{i\bar{i}}} \left[ \frac{1}{2} h\kappa + \kappa h^* - \Delta\rho^* + (1 - \rho)\Delta - i\hbar \frac{d\kappa}{dz} \frac{v_{L,R}}{2} \right]_{i\bar{i}}, \quad (20)$$

with  $v_{L,R}$  the velocity of the left or right fragment in the  $z$  direction (the reaction axis). We can see in Fig. 4 that with this correction the overlap remains almost constant after the reaction.

The results of the corrected neutron pair transfer probability are shown as a function of time in Fig. 5. Despite the efforts to conserve the probability constants after the reaction, small oscillations arise after the reactions. Nevertheless, we expect

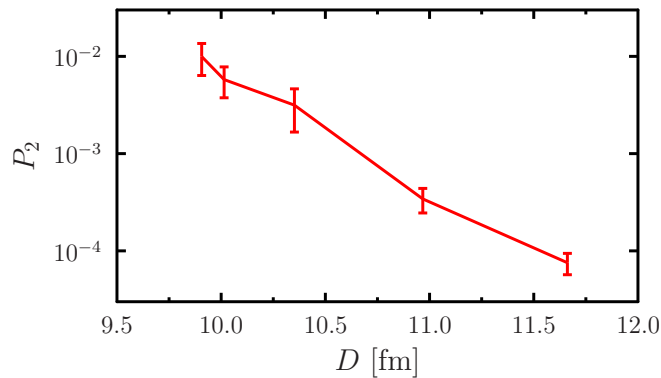


FIG. 6. Neutron pair transfer probability as a function of the distance of closest approach for the reaction  $^{20}\text{O} + ^{20}\text{O}$ .

that the average behavior will fairly reproduce the exact pair transfer probability as it happens in the toy model. Here, let us point out another numerical technique of introducing the chemical potential in Eq. (10). The calculation without the chemical potential and quasiparticle energy is shown also in Fig. 5. As is clearly seen, the transfer probability is not stable after the reaction, illustrating the improving effects of the chemical potential and quasiparticle energy terms in Eq. (10).

We show the neutron pair transfer probability for the reaction  $^{20}\text{O} + ^{20}\text{O}$  as a function of the distance of closest approach [35] in Fig. 6. We see that the pair transfer probability varies almost exponentially with the distance of closest approach. A remarkable point is the absence of individual transfer. The probability to transfer one neutron is smaller than  $10^{-4}$  for all the calculations of the reaction  $^{20}\text{O} + ^{20}\text{O}$  which were carried out in this paper. This reaction is an extreme case where the transfer is only due to the Josephson effect. In Fig. 7, we compare the results obtained by using TDHFB with that using TDHF. In the case of TDHF, the dominant transfer probability is the one neutron, and the pair transfer probability is close to  $P_1^2/4$ , which is the expected value assuming uncorrelated particles [36].

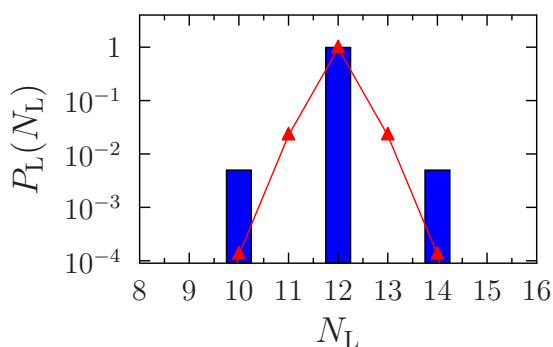


FIG. 7. Probabilities to obtain  $N_L$  neutrons on the left part ( $Z < 0$ ) of the lattice after the collision computed with pairing (blue bars) and without pairing (red triangles) for the reaction  $^{20}\text{O} + ^{20}\text{O}$  at  $E_{\text{c.m.}} = 9.31$  MeV.

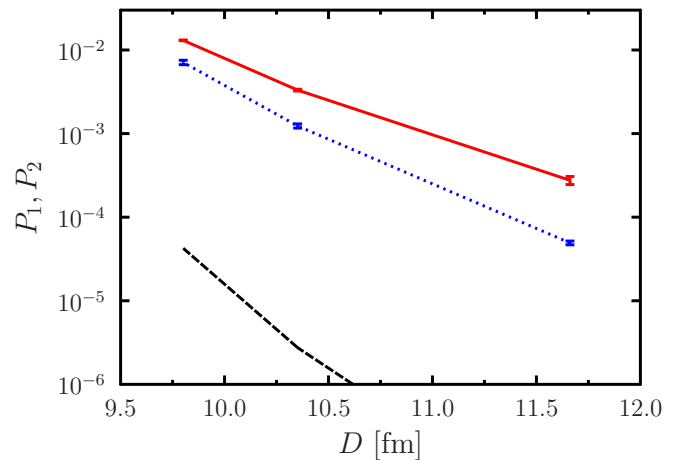


FIG. 8. Transfer probability of one (red solid line) and two neutrons (blue dotted line) as a function of the distance of closest approach for the reaction  $^{14}\text{O} + ^{20}\text{O}$ . The dashed black line represents  $P_1^2/4$ .

In the case with superfluidity, the pair transfer is purely simultaneous. The absence of individual neutron transfer may be due to the large negative  $Q$  value for one-neutron transfer  $Q_{1n} = -3.8$  MeV while the pair transfer  $Q$  value is  $Q_{2n} = -0.9$  MeV. Here, the  $Q$  values are computed from the experimental masses because the determination of the theoretical  $Q$  value is complicated by the need to compute nuclei with odd-particle numbers.

The second case studied is the reaction  $^{14}\text{O} + ^{20}\text{O}$  in which the asymmetry of the reaction makes the transfer more favorable because of the natural tendency to equilibrate the masses of the fragments. We can see in Fig. 8 the neutron transfer probabilities from the  $^{20}\text{O}$  fragments to the  $^{14}\text{O}$ . A large enhancement factor is found between the pair transfer probability and  $P_1^2/4$ . Note that it is also the expected value in the TDHF calculation without pairing [4]. This enhancement of the pair transfer of about two orders of magnitude implies that in the present calculation the pairing correlations play a large role in the transfer process.

*Summary.* The evolution of a set of HFB states is calculated assuming independent TDHFB evolution. The pair transfer probability is then computed from the mixed states obtained with the particle number projector. This method can be used to restore other symmetries like the initial spherical symmetry for reactions between deformed nuclei. The method is successfully tested on a toy model where it can fairly reproduce the exact solution. The method is then applied to the realistic 3D TDHFB calculations with the Gogny force. Several prescriptions are proposed to obtain a correct behavior of the probability of particle transfer as a function of time after the reaction. The calculation shows a large enhancement of the pair transfer probability. In the case of the  $^{20}\text{O} + ^{20}\text{O}$  the single-neutron transfer probability is completely suppressed, and in the  $^{20}\text{O} + ^{14}\text{O}$  reaction a large enhancement factor arises. With this result, we expect in future calculations to closely reproduce the experimental data for the sub-barrier transfer probabilities in reactions where there is a large enhancement factor [35,37].



*Acknowledgments.* The authors thank the members of the DFT meeting for exciting discussions. The authors thank Professor T. Nakatsukasa for discussions and comments. The authors thank D. Lacroix and D. Regnier for discussion and for pointing out a mistake in the calculation of the

solution of the toy model. This research work is partly supported by the results of HPCI Systems Research Projects (Project ID hp170068). The numerical calculations were partly performed using COMA at the CCS of the University of Tsukuba.

- 
- [1] B. Avez, C. Simenel, and Ph. Chomaz, *Phys. Rev. C* **78**, 044318 (2008).
- [2] S. Ebata, T. Nakatsukasa, T. Inakura, K. Yoshida, Y. Hashimoto, and K. Yabana, *Phys. Rev. C* **82**, 034306 (2010).
- [3] S. Ebata, T. Nakatsukasa, and T. Inakura, *Phys. Rev. C* **90**, 024303 (2014).
- [4] G. Scamps and D. Lacroix, *Phys. Rev. C* **87**, 014605 (2013).
- [5] I. Stetcu, A. Bulgac, P. Magierski, and K. J. Roche, *Phys. Rev. C* **84**, 051309(R) (2011).
- [6] A. Bulgac, P. Magierski, K. J. Roche, and I. Stetcu, *Phys. Rev. Lett.* **116**, 122504 (2016).
- [7] Y. Hashimoto, *Eur. Phys. J. A* **48**, 1 (2012).
- [8] Y. Hashimoto and G. Scamps, *Phys. Rev. C* **94**, 014610 (2016).
- [9] H. Goutte, J. F. Berger, P. Casoli, and D. Gogny, *Phys. Rev. C* **71**, 024316 (2005).
- [10] D. Regnier, N. Dubray, N. Schunck, and M. Verriere, *Phys. Rev. C* **93**, 054611 (2016).
- [11] A. Zdeb, A. Dobrowolski, and M. Warda, *Phys. Rev. C* **95**, 054608 (2017).
- [12] A. S. Umar and V. E. Oberacker, *Phys. Rev. C* **74**, 061601 (2006).
- [13] A. S. Umar, V. E. Oberacker, and C. Simenel, *Phys. Rev. C* **92**, 024621 (2015).
- [14] R. Balian and M. Vénéroni, *Phys. Lett. B* **136**, 301 (1984).
- [15] J. M. A. Broomfield and P. D. Stevenson, *J. Phys. G* **35**, 095102 (2008).
- [16] C. Simenel, *Phys. Rev. Lett.* **106**, 112502 (2011).
- [17] C. Simenel, *Eur. Phys. J. A* **48**, 152 (2012).
- [18] S. Ayik, *Phys. Lett. B* **658**, 174 (2008).
- [19] S. Ayik, K. Washiyama, and D. Lacroix, *Phys. Rev. C* **79**, 054606 (2009).
- [20] K. Washiyama, S. Ayik, and D. Lacroix, *Phys. Rev. C* **80**, 031602(R) (2009).
- [21] B. Yilmaz, S. Ayik, D. Lacroix, and K. Washiyama, *Phys. Rev. C* **83**, 064615 (2011).
- [22] Y. Tanimura, D. Lacroix, and S. Ayik, *Phys. Rev. Lett.* **118**, 152501 (2017).
- [23] P. Magierski, K. Sekizawa, and G. Wlazłowski, *Phys. Rev. Lett.* **119**, 042501 (2017).
- [24] K. Sekizawa, G. Wlazłowski, and P. Magierski, *arXiv:1705.04902*.
- [25] A. Bulgac and S. Jin, *Phys. Rev. Lett.* **119**, 052501 (2017).
- [26] C. Simenel, *Phys. Rev. Lett.* **105**, 192701 (2010).
- [27] K. Sekizawa and K. Yabana, *Phys. Rev. C* **88**, 014614 (2013); *ibid.* **90**, 064614 (2014).
- [28] Sonika *et al.*, *Phys. Rev. C* **92**, 024603 (2015).
- [29] G. Scamps, C. Rodriguez-Tajes, D. Lacroix, and F. Farget, *Phys. Rev. C* **95**, 024613 (2017).
- [30] V. N. Fomenko, *J. Phys. A: Gen. Phys.* **3**, 8 (1970).
- [31] C. Simenel, *J. Phys. G: Nucl. Part. Phys.* **41**, 094007 (2014).
- [32] G. Scamps and Y. Hashimoto, *arXiv:1704.00930*.
- [33] G. F. Bertsch and L. M. Robledo, *Phys. Rev. Lett.* **108**, 042505 (2012).
- [34] P. Ring and P. Schuck, *The Nuclear Many-Body Problem* (Springer, Berlin, 1980).
- [35] L. Corradi *et al.*, *Phys. Rev. C* **84**, 034603 (2011).
- [36] K. Hagino and G. Scamps, *Phys. Rev. C* **92**, 064602 (2015).
- [37] D. Montanari *et al.*, *Phys. Rev. Lett.* **113**, 052501 (2014).